AIAA JOURNAL
Vol. 34, No. 4, April 1996

Numerical Simulations of Transitional Axisymmetric Coaxial Jets

M. V. Salvetti*
University of Pisa, 56126 Pisa, Italy
and
P. Orlandi† and R. Verzicco‡
University of Rome "La Sapienza," 00184 Rome, Italy

Direct numerical simulations of spatially evolving axisymmetric coaxial jets are carried out using nonreflecting radiative boundary conditions at the outflow. The sensitivity of the numerical solution to the domain size is investigated, pointing out the feedback effect of the boundary conditions on the pressure at the inlet. The effects of the Reynolds number on the characteristics of the flow are studied. In the initial phase following an impulse, the evolution of the startup vortex is found to be independent of the Reynolds number, whereas the circulation per unit length at the vortex center increases with the Reynolds number. The Reynolds number is also found to affect the further development of the shear-layers' instabilities. Finally, the effects of the inlet conditions on the dynamics of vortical structures are investigated. Two simulations are carried out, in which the inlet velocity profile is unperturbed and perturbed randomly, and the results are compared with flow visualizations from experiments. In the unperturbed case the rollup of the external shear layer occurs at a much larger distance from the jets exit than in experiments, whereas in the perturbed case a good agreement with the experiments is obtained.

I. Introduction

THE flow originated by coaxial jets is of great interest from the perspective of aeronautical and industrial applications. Much of the aeronautical interest is related to noise reduction achievable by coaxial jets in comparison with simple jets. The effect of noise reduction by the addition of a surrounding coaxial stream to a single jet has been observed by several authors (for instance, see Ref. 1). It has been suggested that the aerodynamic noise generated by simple and coaxial jets is related to the dynamics of large-scale vortical structures forming from the instability of the shear layers.[2,3] The prediction and control of these structures by external forcing are necessary to have a better mixing between streams. This could be useful in industrial applications, for example, the design of new industrial burners for efficient combustion and minimum pollution. Large vortical structures play a role mainly in the initial region, where the azimuthal disturbances, if not intentionally introduced, do not have sufficient time to grow and influence the dynamics of the jets.

Although the flow originated by coaxial jets has been studied by hot wire, laser measurements, and flow visualizations,[4–9] the amount of information presently available on the dynamics and the characteristics of large-scale structures is far from exhaustive.

Direct numerical simulations, although restricted to low Reynolds numbers, provide quantities, for instance, pressure and vorticity that are difficult or impossible to get from real experiments. Moreover, numerical simulations permit the control of initial and boundary conditions and the investigation of their effects on the dynamics of the flow. Thus, numerical simulation is a complementary tool that with experimentation provides for a satisfactory understanding of the dynamics of coaxial jets. To our knowledge, in the literature, there are no fully resolved direct numerical simulations of spatially evolving coaxial jets because of computer limitations.

The present axisymmetric numerical simulations contribute to the study of the transitional zone, extending over a few diameters after the jets' exit. These simulations are a first step to check a numerical method that can be easily extended to three-dimensional simulations, currently difficult to perform because of computer limitations. Three-dimensional simulations, however, require boundary conditions that can be studied in the axisymmetric approximation, and the main goal of this research is to investigate the influence of inlet conditions on the dynamics of coaxial jets. We also determine if simple radiative outflow conditions are suitable for this type of simulation. The assumption of axisymmetry is justified in the initial region since it has been observed from experiments that the structures forming from the rollup of the shear-layers remain axisymmetric over a distance of few diameters.[7]

The velocity profile at the inlet has been specified to reproduce one of the conditions of the low Reynolds number experiments in Ref. 7. To simulate the spatial evolution of the flow within a limited axial length, radiative conditions have been applied at the outlet boundary of the computational domain.[10] In the direct simulations of unsteady separated boundary layers in Ref. 11, it has been shown that these types of conditions allow the vortical structures generated in the domain to be convected out of the boundary without a significant distortion. We choose these conditions, from among others proposed in the literature, because of their simplicity. The sensitivity of the solutions to the size of the computational domain has been studied, showing the effect of the outlet boundary conditions on the dynamics of the flow.

The effect of the Reynolds number on the dynamics of the structures has been also investigated in the initial phase following the impulsive startup and when the flow has reached its final regime.

Finally, the effects of the inlet conditions on the formation and dynamics of the vortical structures are investigated. Indeed, two numerical simulations are carried out, in which the inlet velocity profile was unperturbed and perturbed randomly. The numerical flow visualizations have been compared to the experimental ones.[7]

II. Governing Equations and Numerical Method

The axisymmetric Navier–Stokes equations in primitive variables and in cylindrical coordinates are used. The unknowns are $q_r = rv_r$, $q_z = v_z$, and the pressure p, where v_r and v_z are the radial and the axial velocity components, respectively. The continuity equation with these variables is

$$\frac{\partial q_r}{\partial r} + r\frac{\partial q_z}{\partial z} = 0 \tag{1}$$

Received May 3, 1995; revision received Nov. 15, 1995; accepted for publication Nov. 20, 1995.

*Assistant Professor, Dipartimento di Ingegneria Aerospaziale, V. Diotisalvi 2.
†Professor, Dipartimento di Meccanica e Aeronautica, V. Eudossiana 18.
‡Assistant Professor, Dipartimento di Meccanica e Aeronautica, V. Eudossiana 18.

and the momentum equations in conservative form are

$$\frac{\partial q_r}{\partial t}+\frac{\partial}{\partial r}\left(\frac{q_r^2}{r}\right)+\frac{\partial q_r q_z}{\partial z}=-r\frac{\partial p}{\partial r}+\frac{1}{Re}\left[r\frac{\partial}{\partial r}\left(\frac{1}{r}\frac{\partial}{\partial r}q_r\right)+\frac{\partial^2 q_r}{\partial z^2}\right] \quad (2)$$

$$\frac{\partial q_z}{\partial t}+\frac{1}{r}\frac{\partial q_r q_z}{\partial r}+\frac{\partial q_z^2}{\partial z}=-\frac{\partial p}{\partial z}+\frac{1}{Re}\left[\frac{1}{r}\frac{\partial}{\partial r}\left(r\frac{\partial}{\partial r}q_z\right)+\frac{\partial^2 q_z}{\partial z^2}\right] \quad (3)$$

To have flow visualizations, as in the experiments, the transport equation for a passive scalar is introduced:

$$\frac{\partial \Theta}{\partial t}+\frac{1}{r}\frac{\partial q_r \Theta}{\partial r}+\frac{\partial q_z \Theta}{\partial z}=\frac{1}{ReSc}\left[\frac{1}{r}\frac{\partial}{\partial r}\left(r\frac{\partial \Theta}{\partial r}\right)+\frac{\partial^2 \Theta}{\partial z^2}\right] \quad (4)$$

where Θ is the concentration of the passive scalar, the Schmidt number $Sc = \nu/D$, where ν is the kinematic viscosity and D the diffusivity of the scalar.

The equations have been nondimensionalized using the radius of the internal jet R_i as a length scale, and the centerline axial velocity V_i as a velocity scale; hence, the Reynolds number is $Re = V_i R_i/\nu$.

The spatial discretization of the system of equations (1–4) is performed by centered finite differences, second-order accurate. The variables are located on a staggered grid with the pressure at the center of the cell and the q_i at the cell faces. The use of staggered grids, together with the choice of the variables q_i, simplifies the discretization at the axis ($r = 0$), where the governing equations are singular. Indeed, the advantage of using staggered grids is that only the component q_r is evaluated at the grid point $j = 1 (r = 0)$; since at that point $q_r = 0$ by definition, it is not necessary to discretize the equation for q_r at $r = 0$. The equation for q_z requires the evaluation of radial derivatives in the region around the axis. The fact that $q_r = 0$ at $j = 1$ avoids the evaluation of q_z at $j = 1$, and the radial derivative in the convective terms can be discretized without any approximation. The discretization of the viscous radial derivative described in Ref. 12 mantains second-order accuracy near the axis.

The advancement in time is carried out by a fractional-step method,[13] in which as a first step an intermediate nonsolenoidal velocity field $\hat{q}_i$ is provisionally calculated. Then it is projected into a solenoidal one by a scalar quantity Φ. The pressure is related to the scalar Φ. The third-order Runge–Kutta scheme described in Ref. 14 is used to advance the momentum equations in time, in which nonlinear terms are computed explicitly and linear terms implicitly. Using an approximate factorization technique, the inversion of a large sparse matrix is approximated by inversion of tridiagonal matrices. The method consists of three substeps, and at each substep the scalar Φ is calculated. The computation of Φ implies the solution of an elliptic equation for which trigonometric expansions are applied in the axial direction. This procedure, together with the inversion of a tridiagonal matrix, is very efficient to calculate Φ directly and gives the solenoidal velocity field within roundoff errors.

Nonuniform grids in r were used to cluster the points in high-shear regions by the following coordinate transformation:

$$r_j = R_0 \eta(x_j)$$

where r_j is the radial coordinate of the point j; also, R_0 is the radial size of the computational domain and x_j is the computational coordinate corresponding to an uniform distribution of the N points in a [0,1] interval. The function $\eta(x_j)$ is

$$\eta(x_j)=\eta_1(x_j)\left\{\frac{1}{\eta_1(x_N)}+\left(1-\frac{1}{\eta_1(x_N)}\right)\frac{\tanh[\alpha(x_j-1)]}{\tanh[\alpha(\bar{x}-1)]}\right\}$$

$$\eta_1(x_j)=\frac{R_1}{R_0}\frac{\tanh(\alpha x_j)}{\tanh\alpha}$$

where α, R_1, and $\bar{x}$ are parameters determining the zone of clustering of the computational points, set to 4, 1.6, and 0.65, respectively.

Because of the use of trigonometric expansions in the computation of Φ, the grid must be uniform in the z direction.

III. Boundary Conditions

In the numerical simulation, boundary conditions must be assumed, and these must reproduce as closely as possible the experimental conditions.

At the external radial boundary, free-slip conditions are assumed. Since we are interested in simulating freejets, the radial extension of the computational domain must be large enough to prevent the free-slip conditions from affecting the entrainment. The importance of the location of the radial boundary is not just a peculiarity of the numerical simulations; in fact, it was also observed in laboratory experiments that the dynamics of the jet is affected by the location of the physical external confinement. To prove the sensitivity to the location of the radial boundary, two simulations were performed for a single jet in Ref. 15, with the radial size equal to $5R$ and $3R$ (R is the radius of the jet) at $Re = 2000$. In the first case, the initial instabilities as a result of the impulsive startup die out; whereas, in the second case, they are sustained. The same qualitative effect was observed for coaxial jets, but we are not presenting the results of this study in the present paper. Nevertheless, it has been verified that the radial dimension of the domain in the present simulations is large enough to avoid the effects of free-slip conditions at the external radial boundary on the dynamics of the jet (see Sec. IV.A). On the other hand, the sensitivity of the solution to the axial length of the domain has been studied, and the results are presented as follows.

At the inlet of the computational domain, the axial velocity is set to zero at $t = 0$ and evolves to a prescribed profile $Q_z(r)$ in a time τ,

$$q_z(t,r) = f(t)Q_z(r) \quad t<\tau; \quad f(t) = 3(t/\tau)^2 - 2(t/\tau)^3 \quad (5)$$

where $Q_z(r)$ is the basic stationary profile. The law for $f(t)$ in Eq. (5), together with a very small value of τ, permits the reproduction of the transient generated by the opening of a valve or the time required for a motor to reach its final speed in an experiment. The impulsive startup of the jet and its initial development was simulated by looking at the evolution of the large vortex forming at the startup. This study is interesting in that it helps to understand the propagation of a flame front and the dynamics of pulsating jets. In all of the simulations the parameter τ in Eq. (5) is equal to 0.4. To compare our results with the visualizations in Ref. 7, the axial velocity profile $Q_z(r)$ at the inlet of the computational domain is chosen to reproduce as closely as possible the experimental profile of case 2 in Ref. 7. By fixing the maximum velocity, the radius, the momentum thickness θ, and displacement thickness δ of the internal and external jet, fifth-order polynomial functions give the basic velocity profile. In the internal and the external shear layers the profiles are approximated by fifth-order polynomials

$$P(x) = ax^5 + bx^4 + cx^3 + dx^2 + ex + f$$

For simplicity we assume here a fictitious coordinate x that varies between 0 and 1. The profiles in the internal and external shear layers are given by the polynomial $P(x)$, using the following changes of variables: $r = s_i(x-1) + R_i$ in the internal shear layer, $r = s_e(1-x) + R_i$ and $r = s_e(x-1) + R_e$ in the shear layers of the external jet. The unknown coefficients in $P(x)$ are obtained imposing the following conditions:

$$P(0) = V_k \qquad V_k = V_i, V_e$$

$$P(1) = 0 \qquad \left.\frac{dP(x)}{dx}\right|_{x=0} = 0$$

$$\int_0^1 \left(1-\frac{P(x)}{V_k}\right)dx = \delta_k \qquad \delta_k = \delta_i, \delta_e$$

$$\int_0^1 \left(1-\frac{P(x)}{V_k}\right)\frac{P(x)}{V_k}dx = \theta_k \qquad \theta_k = \theta_i, \theta_e$$

under the constraint $dP(x)/dx|_{x\to 1} \le 0$. Outside the shear layers the axial velocity is constant. In the present simulations the ratio between the maximum velocity of the internal and the external jet

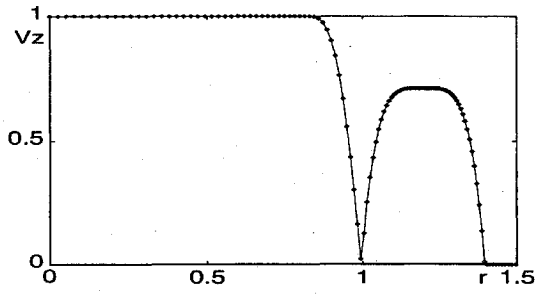

Fig. 1 Axial velocity profile at the inlet.

V_e/V_i is 0.71, and the ratio between the external and internal radius is $R_e/R_i = 1.41$. The momentum and displacement thickness of the internal and external shear layers are, from Ref. 7, $\theta_i = 0.0187R_i$, $\theta_e = 0.0165R_i$, and $\delta_i = 0.0465R_i$ and $\delta_e = 0.0366R_i$, respectively, and s_i and s_e are set equal to $0.175R_i$. In Fig. 1 the axial velocity profile is plotted and the computational points are visible to show the grid spacing in r.

As already mentioned the quantities were nondimensionalized using the internal radius $R_i = 2.73$ cm, the velocity on the axis of the inner jet ($V_i = 11$ cm/s in the simulations at $Re = 3000$), and the kinematic viscosity of water $\nu = 0.01$ cm^2/s.

After the end of the transient different assumptions can be used for the inlet profile; the simplest one is to keep it constant:

$$q_z(t, r) = Q_z(r) \qquad t > \tau \tag{6}$$

This condition, however, does not reproduce the actual experimental conditions, where the inlet velocity profile varies in time, because of the turbulence of the flow at the exit of the nozzle or of the disturbance induced by experimental devices. It is difficult to identify an inlet condition that could account for both of these effects. To reproduce the fluctuations of the inlet velocity profile because of the turbulence in the nozzle as a second case, a perturbation of zero mean value has also been superposed on to the velocity $Q_z(r)$. Since no measurements of the inlet velocity were available in the experiments in Ref. 7, a random perturbation $q_z'(t, r) = g(r)G(t, r)$ has been assumed. The inlet profile then is

$$q_z(t, r) = Q_z(r) + g(r)G(t, r) \tag{7}$$

where $G(t, r)$ is Gaussian white noise in t and r and $g(r)$ is the perturbation intensity accounting for a higher turbulence level near the walls of the nozzle. The analytical expression of $g(r)$ has been derived by fitting an exponential function to the boundary layer rms profile[16] obtained in an experiment described in Ref. 5 at higher Reynolds number than in the experiment we wish to reproduce[7]:

$$g(x) = k(ax)^{(-b)}Q_z(x) \tag{8}$$

Again, a fictitious x coordinate has been introduced ranging between σ (the thickness of the viscous sublayer) and 1. The parameters k and b are set to 0.16723 and 0.89616, respectively, whereas a is equal to 35.2941 and to 88.2353 in the internal and external shear layers, respectively. In the viscous sublayer $g(x)$ is assumed to vary linearly from zero to $g(\sigma)$. Clearly this perturbation does not reproduce the real conditions in the experiments of Ref. 7, but it is useful to have indications of the effects of inlet perturbations on the evolution of the jets. It should be stressed that this disturbance does not account for the turbulent structures of the real incoming boundary layers and that, as a further approximation, the component q_r is set equal to zero at the inlet.

At the outflow, radiation boundary conditions are applied to each variable q_i and to the scalar Θ

$$\frac{\partial q_i}{\partial t} + C\frac{\partial q_i}{\partial z} = 0 \tag{9}$$

where C is a velocity that in the Orlanski[10] assumption depends on the flow itself. In Ref. 10 a procedure is proposed for the computation of the velocity C. In the present study, however, C is assumed constant, and this velocity represents the advection speed of large-scale structures. This assumption leads to simple boundary conditions that have the advantage of automatically satisfying the global conservation of mass. This type of condition has been succesfully used in previous simulations of spatially developing free shear layers,[17] plane wakes, [18] and two-dimensional separating boundary layers.[11] Very recently, this type of boundary condition has been successfully used in the large eddy simulation of turbulent confined coannular jets and turbulent flow over a backward facing step.[19] Moreover in Ref. 11 it was pointed out that the value of C was not critical to the solution, since the same results were obtained with different values. In all of the simulations presented here, C is equal to $0.6V_i$. A simulation carried out with $C = 0.3V_i$ confirmed that the solution is not affected by the value of this constant.

The choice of this kind of boundary condition is only one among many. For instance, Jin and Braza[20] used Eq. (9) with the addition of a viscous term, deriving this condition from a wave equation to match the Navier–Stokes equations on the outlet boundary. In the simulation of a free shear-layer flow, they[20] found that these boundary conditions considerably reduce the feedback noise compared to the commonly used free boundary-layer conditions. Similar boundary conditions were also used by Dai et al.[21] in the large eddy simulation of plane turbulent jet flow. In this case the authors[21] add a viscous term to Eq. (9) to improve the numerical stability. Another possibility is to use the final portion of the computational domain as a buffer region to allow part of the disturbances induced by the outflow to be dissipated.[22] Our aim, however, is to use simple boundary conditions that give stable and acceptable solutions. In this respect, the use of Eq. (9) appears to be appropriate, as will be shown in Sec. IV.A. Concerning the stability, Fig. 2 shows that the pressure remains stable in time; whereas, in contrast, Jin and Braza[20] found that with the free boundary-layer conditions the pressure showed amplified oscillations (Fig. 3a in Ref. 20). Moreover, for the simulations at $Re = 3000$ presented in Sec. IV. C. 2, 32,000 time steps were carried out for the unperturbed case, corresponding to about 60 rollups of the external shear layer, with a maximum Courant–Friedrichs–Lewy (CFL) number of 0.4 and 26,000 time steps for the perturbed case with a maximum CFL number of 0.7. As pointed out also in Ref. 19, in statistically steady flows the boundary condition (9) forces the exit streamline to be parallel to the z axis, with zero mean radial velocity, and this may affect the results in a zone around the exit boundary. This problem could be eliminated by computing C as suggested in Ref. 10. The analysis of the results indicates that the mean radial velocity near the exit is low and that the extent of this zone can be estimated as about $2R_i$. Thus, in the results presented in the following section, the solution in this zone near the exit should be considered from this perspective.

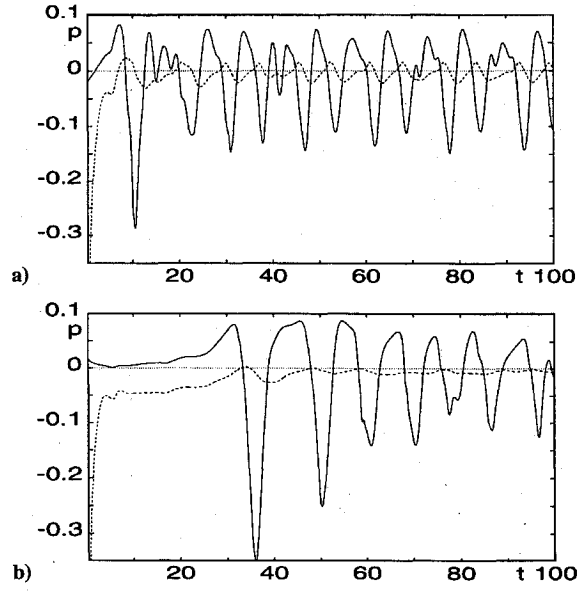

Fig. 2 Time evolution of the pressure at the inlet (- - - -) and at the outlet (——): a) $L_z = 4R_i$ and b) $L_z = 16R_i$.

IV. Results

A. Sensitivity to the Size of the Computational Domain

To investigate the sensitivity of the solution to the axial size of the computational domain, simulations at $Re = 2500$ were carried out for four different axial lengths of $4R_i$, $8R_i$, $12R_i$, and $16R_i$. The radial dimension was $L_r = 5R_i$. Equally spaced grids with 193 points in the radial direction and 97, 193, 289, and 385 points in the axial direction were used.

The vorticity field at $t = 20$, obtained with domain sizes of $8R_i$ and $16R_i$ (Fig. 3), shows that the initial stage of the development of the flow is not affected by the size of the computational domain. For the simulation with $L_z = 8R_i$, the large vortex, formed after the startup, is in the process of leaving the computational domain. This result confirms that the radiative boundary conditions at the outlet of the computational domain effectively allow the vortical structures to exit from the domain without any appreciable reflection or distortion.

On the other hand, at a later time when the flow has reached its final regime, the results for each simulation are different. In particular, the vorticity field in Fig. 4 shows that the rollup of the external shear layer occurs at a smaller distance from the inlet when the domain size is smaller. This behavior can be explained by the fact that the boundary conditions at the outlet affect the pressure at the inlet by a feedback mechanism, as observed for mixing layers in Ref. 23.

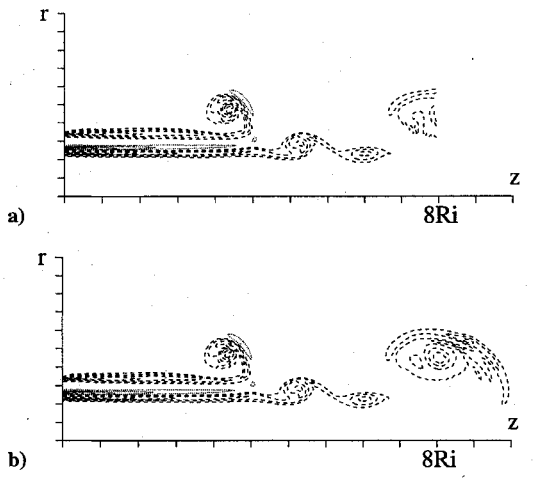

Fig. 3 Isocontours of vorticity for $Re = 2500$ at $t = 20$: a) $L_z = 8R_i$ and b) $L_z = 16R_i$.

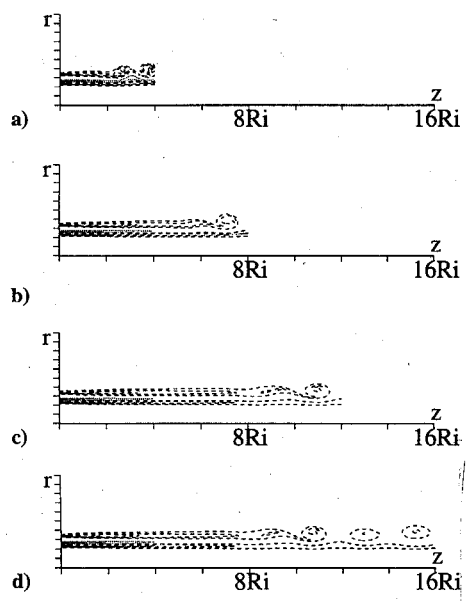

Fig. 4 Isocontours of vorticity for $Re = 2500$ at $t = 200$: a) $L_z = 4R_i$, b) $L_z = 8R_i$, c) $L_z = 12R_i$, and d) $L_z = 16R_i$.

To illustrate this effect, in Figs. 2a and 2b the time evolution of the pressure at the inlet and at the outlet, at $r = 1.3R_i$ (in the external shear layer), is presented for the computations with a domain size of $4R_i$ and $16R_i$, respectively. When a vortical structure reaches the outlet boundary, the pressure decreases to assume a local minimum. The first minimum is observed when the center of the startup vortex crosses the boundary. At the same time, the pressure at the inlet also varies, assuming a local maximum. Since in the inlet region no vortical structures are present and the vorticity field is steady, these oscillations are mainly the result of the feedback from the outlet boundary. Although the peaks in the outlet pressure are of the same order for both of the cases, when the domain is shorter the pressure oscillations at the inlet are stronger. Moreover, each vortical structure takes less time to reach the outlet boundary as the domain is shorter and, hence, the peaks in the inlet pressure occur at a higher frequency. Thus, the feedback from the outlet results in a perturbation of the pressure at the inlet, which has larger amplitude and higher frequency because the domain is shorter. When the domain size is small, this perturbation affects the dynamics of the flow and, in particular, the rollup of the external shear layer occurs closer to the inlet. On the other hand, when the axial size of the computational domain is large enough, the effect of the pressure perturbation on the dynamics of the flow is negligible. The results obtained in the simulation with a length of $12R_i$ are practically identical to those obtained with a size of $16R_i$, as shown in the isocontours of the vorticity presented in Figs. 4c and 4d.

Analogously, it was checked that a radial dimension of the domain of $5R_i$ is large enough to avoid the free-slip conditions at the external radial boundary affecting the entrainment of the jets, as mentioned in Sec. III. Indeed, two simulations were carried out at $Re = 3000$ with L_r equal to $5R_i$ and $8R_i$, respectively, and the results are not significantly different. Hence, we use $L_r = 5R_i$ in all of the simulations presented in the following sections.

B. Initial Development of the Flow

The initial stage of the development of the flow, after the impulsive startup, and in particular the evolution of the large startup vortex, help in understanding the propagation of a flame front or the behavior of a pulsating jet. To investigate the effects of the Reynolds number on this stage of the flow, simulations have been carried out for Reynolds numbers $Re = 500$, 1000, 1500, 2000, 2500, and 3000. As already observed, although the final regime of the jet depends on the axial extension of the computational domain, the initial development of the flow is independent of the length of the domain; therefore, all of the simulations have been performed with $L_z = 8R_i$, using a 193×193 grid.

In Fig. 5 the azimuthal vorticity at $t = 10$, for $Re = 1000$, 2000, and 3000, shows that a large startup vortex forms and its center position is the same in all of the cases. For $Re = 3000$ the external shear layer shows a rollup that does not occur at $Re = 1000$. In Fig. 6 the vorticity fields are presented at a later stage of the development of the flow ($t = 20$). For all of the Reynolds numbers, the startup vortex exits from the domain, and the vorticity distribution in the inner and outer shear layers depends on the Reynolds number. For $Re = 1000$ the external shear-layer rollup is weak; whereas for higher Reynolds numbers, the instability of the external shear layer is more intense. For $Re = 3000$ a second rollup of the internal shear layer is also noticeable.

From qualitative observations of the vorticity field the position of the startup vortex seems to be independent of the Reynolds number. To better investigate this point and to have quantitative information, we determine the position of the center of the vortices by use of a criterion based on the eigenvalues of the velocity gradient tensor, as proposed in Ref. 24. The velocity gradient tensor for axisymmetric flows is

$$\Delta V = \begin{pmatrix} \dfrac{\partial v_z}{\partial z} & \dfrac{\partial v_z}{\partial r} & 0 \\ \dfrac{\partial v_r}{\partial z} & \dfrac{\partial v_r}{\partial r} & 0 \\ 0 & 0 & \dfrac{v_r}{r} \end{pmatrix}$$

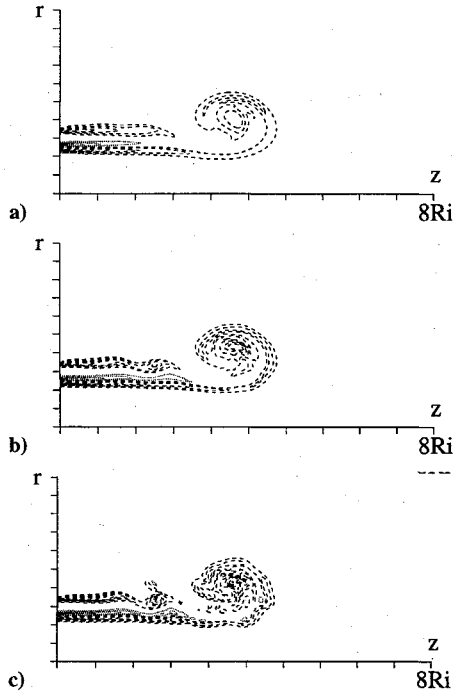

Fig. 5 Isocontours of vorticity, $t = 10$: a) $Re = 1000$, b) $Re = 2000$, and c) $Re = 3000$.

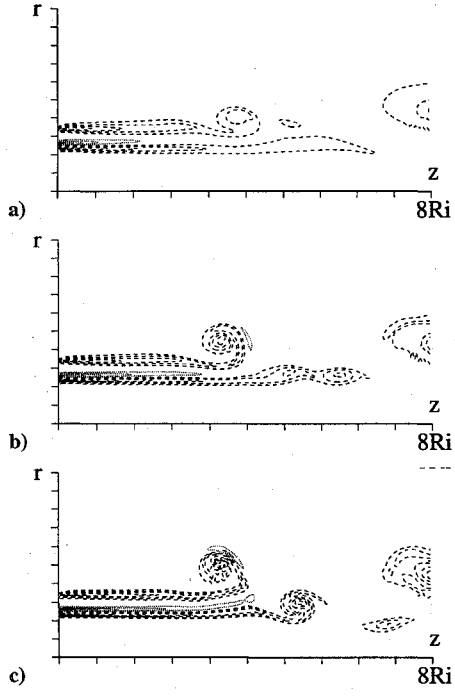

Fig. 6 Isocontours of vorticity, $t = 20$: a) $Re = 1000$, b) $Re = 2000$, and c) $Re = 3000$.

The eigenvalues being complex implies the existence of a local spiral/circular pattern of streamlines in the neighborhood of the point considered. The boundary of the region with the complex eigenvalues is obtained from the discriminant of the cubic characteristic equation $\det(\Delta V - \lambda I) = 0$. A real eigenvalue is clearly $\lambda_1 = v_r/r$. Thus, the other eigenvalues can be obtained from the following quadratic equation:

$$\lambda^2 + B\lambda + C = 0$$

where

$$B = -\left(\frac{\partial v_r}{\partial r}\right) - \left(\frac{\partial v_z}{\partial z}\right)$$

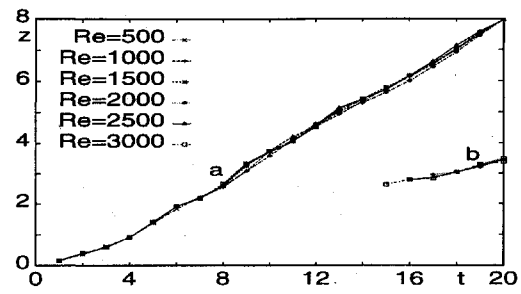

Fig. 7 Position of the minimum of Δ for different Reynolds numbers.

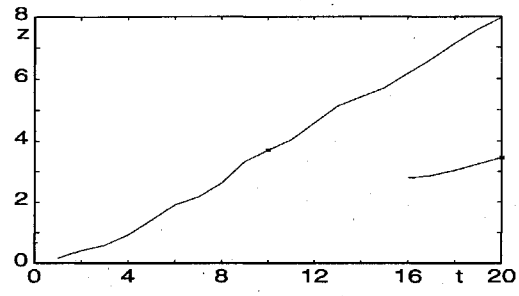

Fig. 8 Position of the minimum of Δ for different grids at $Re = 2500$.

and

$$C = \left(\frac{\partial v_z}{\partial z}\right)\left(\frac{\partial v_r}{\partial r}\right) - \left(\frac{\partial v_r}{\partial z}\right)\left(\frac{\partial v_z}{\partial r}\right)$$

Complex eigenvalues occur when the discriminant $\Delta = B^2 - 4C < 0$. In Fig. 7 the axial position of the minimum of Δ is plotted as a function of the time, for different Reynolds numbers. At the initial stage of the development of the flow, the minimum has the same position for all of the Reynolds numbers, meaning that the formation and the convection of the startup vortex is independent of the Reynolds number (see lines a, Fig. 7). The evolution in time of the position of this vortex, identified by a local minimum of Δ, is the same for all of the Reynolds numbers (last part of lines a, Fig. 7). Nevertheless, for high Reynolds numbers, at a certain time, the minimum of Δ is found closer to the inlet of the jets than the star-tup vortex (lines b, Fig. 7). This corresponds to the vortex forming from the rollup of the external shear-layer (e.g., see Figs. 6b and 6c). The rollup of the external shear layer occurs earlier and closer to the inlet as the Reynolds number increases.

The grid independence of the results was checked at $Re = 2500$, by doubling the grid points in the axial direction. The axial positions of the minimum of Δ obtained at different times with the finer grid ($*$ symbols in Fig. 8) are almost undistinguishable from those obtained with the coarser grid (solid line in Fig. 8).

The fundamental role played by large vortical structures in the entrainment and mixing has been pointed out in the literature. In particular, in the formation of an axisymmetric vortex ring[25] the mixing is proportional to the vortex circulation. In Fig. 9 the circulation of the vorticity per unit axial length is plotted vs the axial coordinate, at different times and at $Re = 1000$, 2000, and 3000. The maximum of the circulation coincides with the axial position of the center of the startup vortex that at the times presented in Fig. 9 is moving toward the outlet boundary. The circulation peak increases with the Reynolds number. A further local maximum of the circulation is found connected with the rollup of the external shear layer. In accordance with the remarks made when discussing Fig. 6, the peak of the circulation corresponding to this vortex center shows a higher dependence on the Reynolds number. At $Re = 2000$ and 3000 it is interesting to remark that negative values of the circulation are found immediately after the external shear-layer vortex. This opposite sign circulation is because of negative vorticity originated from the internal shear-layer of the external jet and advected by the vortex from the external shear layer as shown in Fig. 6.

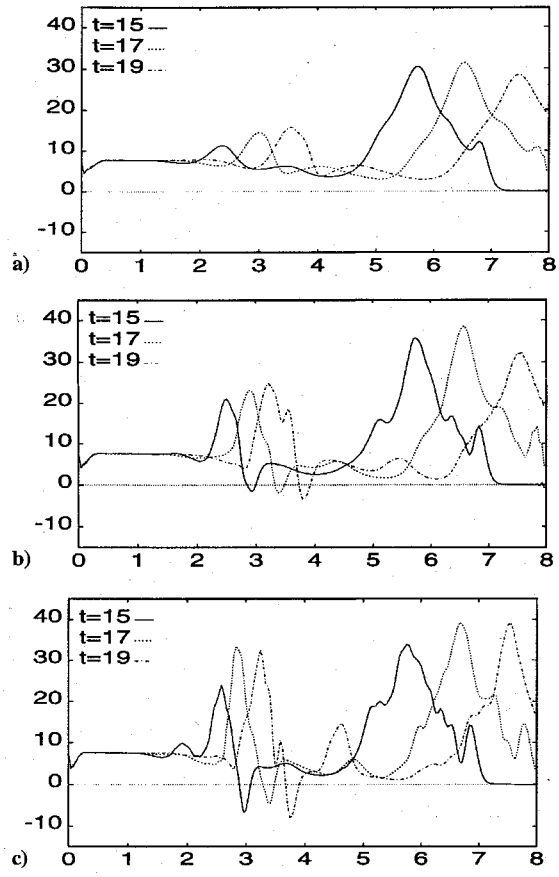

Fig. 9 Per unit length circulation at different times: a) Re = 1000, b) Re = 2000, and c) Re = 3000.

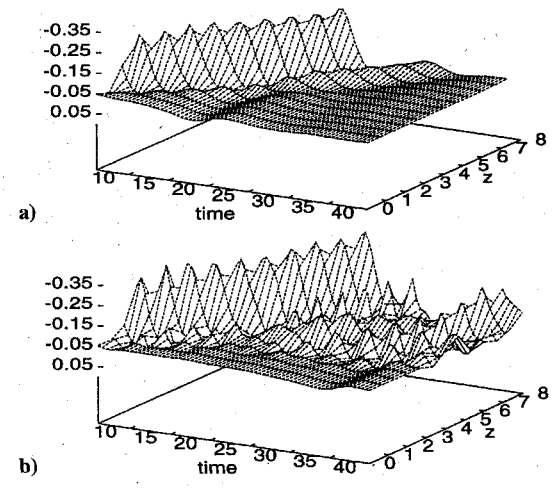

Fig. 10 Time evolution of the distribution of pressure in axial direction in the external shear layer: a) Re = 500 and b) Re = 3000.

C. Analysis of the Flow Dynamics

1. Sensitivity to the Reynolds Number

The development of the flow after the initial phase depends on the Reynolds number. Indeed, for low Reynolds numbers the instabilities of the shear layers, initiated by the impulsive startup, are not sustained, and a steady state is reached. As an example, since vortex centers correspond to local pressure minima, in Fig. 10a the pressure is plotted as a function of time and z at $Re = 500$ and $r = 1.3R_i$. Two local minima of pressure can be observed: the higher corresponds to the large startup vortex, whereas the other one corresponds to a second vortex forming from the external shear layer triggered by the startup vortex. As time increases, the pressure fluctuations are reduced, meaning that no more vortices form and a

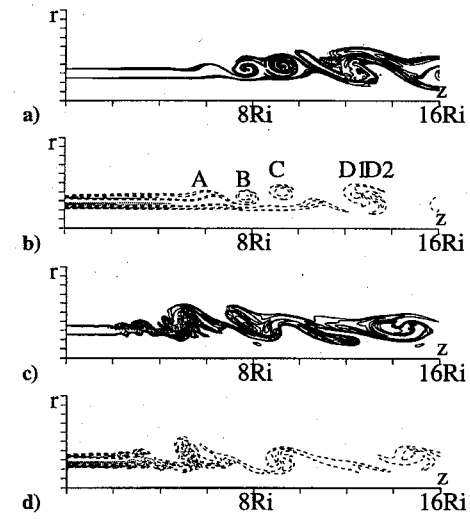

Fig. 11 Passive scalar concentration and vorticity field at t = 206: a) unperturbed case, isocontours of passive scalar concentration, b) unperturbed case, isocontours of vorticity, c) perturbed case, isocontours of passive scalar concentration, and d) perturbed case, isocontours of vorticity.

steady state is reached. Conversely, at $Re = 3000$ Fig. 10b shows that vortices continuously form from the instability of the external shear layers, and the flow is characterized by the rollup and pairing of these vortices.

2. Comparison with the Experiments

The final goal of this research was the numerical simulation of the flow at $Re = 3000$, since at this Reynolds number a comparison with the flow visualizations for case 2 in Ref. 7 is possible; then the validation of the numerical method can be performed. On the basis of the preceding considerations, the axial length of the computational domain has been set equal to $16R_i$. The grid has 193 and 385 points in radial and axial directions, respectively.

A first simulation was carried out without any perturbation of the inlet velocity profile. The vorticity field in Fig. 11b shows the formation of vortical structures (B and C) from the rollup of the external shear layer. These vortices are advected downstream until they pair (this is not visible in Fig. 11b). The resulting vortical structure pairs downstream with that formed from the rollup of the internal shear layer, as D1 and D2 in the figure. Although the dynamics of the flow is characterized by the repetition of such events, the flow is not perfectly periodic, probably because of the interactions between instabilities of the internal and external shear layers. The distributions of a passive scalar, having a concentration at the inlet equal to 1 in the external jet and equal to 0 elsewhere, were compared to the sequence of visualizations reported in Ref. 7. The distribution of the passive scalar and the vorticity field at $t = 206$ in Figs. 11a and 11b show that in the numerical simulation the rollup of the external shear layer occurs at a distance from the inlet of about $6R_i$, whereas in the experiment it was found at a distance of about $2R_i$. Possible explanations for this discrepancy have been examined. Namely, the enhanced stability of the external shear layer in the numerical simulation could be because of the assumption of axial symmetry. Nevertheless, as discussed earlier, this assumption agrees with the experimental observations in the initial region. In our opinion, this discrepancy is because in the numerical simulation the inlet velocity profile does not have any temporal perturbation. On the other hand, in all experiments the inlet profile exhibits fluctuations in time, because of the turbulent character of the flow at the exit of the nozzle or because of perturbations introduced by the experimental devices. The effect of the turbulent wall structures forming in the test section is important, but, since the axisymmetric assumption was made, these can not be introduced.

A reasonable way to introduce the effects of turbulence is by a random perturbation, such as that given in Eq. (7), superimposed to the inlet velocity profile. Even if a random perturbation does not reproduce the actual conditions of the experiments in Ref. 7,

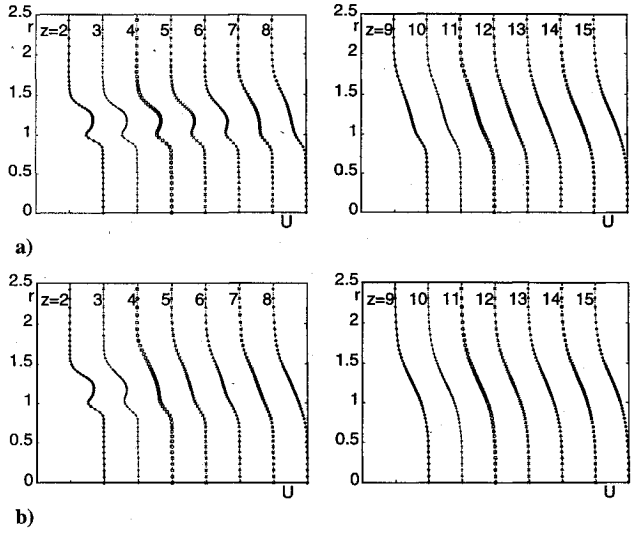

Fig. 12 Radial profiles of mean axial velocity: a) unperturbed case and b) perturbed case.

a better agreement with the experimental observations is obtained. Indeed, the rollup of the external shear layer occurs approximately at a distance of $2R_i$ from the inlet, as shown by the instantaneous picture of the passive scalar concentration in Fig. 11c. As in the experimental visualizations in Fig. 7 of Ref. 7, a second rollup of the external shear layer is observed immediately after the first one. Larger structures are observed downstream. The vorticity field in Fig. 11d shows that these are the result of the pairing of the vortices from the external shear layer, and also of their pairing with the structures from the internal shear-layer, that in this simulation rollup in the same zone as the external one. Nevertheless, the comparison with the experiments is possible only in the initial region, because of the axisymmetric assumption made in the simulations. To prove that the position of the initial rollup does not depend on the amplitude of the inlet perturbation, a simulation was carried out with the random perturbation twice as large, and the rollup of the external shear layer occurred at the same distance from the inlet.

The profiles of time-averaged axial velocity in Figs. 12a and 12b show that in the perturbed case the outer potential core, i.e., the zone after the jet exit where the time-averaged streamwise velocity is equal to V_e, ends at $z/R_i = 2$; whereas in the unperturbed case, it ends at a distance of $5R_i$ from the exit of the nozzle. This behavior confirms the earlier considerations on the distribution of the passive scalar. Moreover, in the perturbed simulation, the velocity profile takes a shape of a single jet at $z/R_i = 8$, whereas in the unperturbed case at $z/R_i = 12$, suggesting that the mixing between the layers occurs closer to the inlet in the perturbed case. For both of the simulations, the inner potential core, given by the region after the jet exit where the time averaged v_z is equal to V_i, persists all over the length of the computational domain. This result does not agree with experiments, in which the end of the inner potential core was estimated at about $8R_i$ beyond the jet exit. This discrepancy is probably because of the assumption of axial symmetry in the simulation. Indeed, the three-dimensional mechanisms, occurring mainly because of azimuthal instabilities, have been shown in temporally evolving mixing layers[26,27] to play a fundamental role in transition to turbulence and in circular jets[28] to produce a greater spreading of the jet. Indeed, in Ref. 28 it is shown that in the three-dimensional case there is a hierarchy of counter-rotating axial vortices that extend all of the way radially up to the axis of symmetry. These structures penetrate deeply into the potential core of the jet causing its erosion. Therefore, the lack of these mechanisms in the present axisymmetric simulations causes an enhanced stabililty of the inner potential core.

As discussed before, the assumption of axisymmetry is expected to also affect the spreading of the jets. Indeed, from Figs. 12a and 12b, the spreading seems to be important only in a region extending a few diameters after the rollup of the external shear layer, for both the unperturbed and the perturbed simulations, whereas in experiments, the spreading is observed over a greater length. The radial dimension of the jet at the exit of the computational domain in the perturbed and unperturbed case is comparable (see Fig. 12).

V. Conclusions

Numerical simulations of spatially evolving axisymmetric coaxial jets have been carried out, as a first step to check a numerical method that can be easily extended to three-dimensional simulations. These more realistic simulations are not possible at the moment because of computer limitations. However, the numerical boundary conditions required in these simulations can be studied in the axisymmetric approximation. The main goal of this research is to investigate the influence of inlet conditions on the dynamics of coaxial jets. Another point of interest is to study whether simple radiative conditions are suitable for these types of flows.

Simulations with different lengths of the computational domain showed that the radiative boundary conditions at the outlet effectively allow the vortical structures to leave the domain without any significant distortion or reflection. Nevertheless the boundary conditions have been found to affect the dynamics of the jets, through a feedback effect by the pressure field. This feedback becomes negligible as the axial size of the computational domain increases.

The Reynolds number clearly affects the flow. We decided to study separately the Reynolds number effects in the initial phase after the impulsive startup and in the full regime. The evolution of the large startup vortex was found to be independent of the Reynolds number, whereas the circulation per unit length at the center of this vortex increases with the Reynolds number. The dynamics of the flow after the initial phase, on the other hand, is dependent on the Reynolds number: for low Reynolds number a steady state was reached, whereas for high Reynolds number an unsteady aperiodic motion was obtained.

To check the sensitivity to the inlet conditions, two simulations were carried out at $Re = 3000$, with and without a random perturbation superimposed to the basic velocity profile at the inlet. This random perturbation is given to obtain inlet conditions closer to those in experiments on unexcited coaxial jets. The comparison with the flow visualizations of case 2 in Ref. 7 pointed out the importance of the inlet conditions on the formation and dynamics of the vortical structures. Indeed, in the unperturbed case the rollup of the external shear layer occured at a larger distance from the nozzle exit than in experiments, whereas in the perturbed case this distance is comparable to the experimental one. The inlet conditions also affect the length of the outer potential core and the mixing between the layers. Nevertheless, discrepancies with the experiments are observed, because of the assumption of axisymmetry, which is justified only in the initial zone. Indeed, a longer inner potential core and less spreading than in experiments are observed in both of the simulations.

References

[1]Williams, T. J., Ali, M. R. M. H., and Anderson, J. S., "Noise and Flow Characteristics of Coaxial Jets," *Journal of Mechanical Engineering Science*, Vol. 2, 1969, p. 133.

[2]Hussain, A. K. M. F., "Coherent Structures and Turbulence," *Journal of Fluid Mechanics*, Vol. 173, Dec. 1986, p. 303.

[3]Roshko, A., "Structure of Turbulent Shear Flows: A New Look," *AIAA Journal*, Vol. 14, No. 10, 1976, p. 1349.

[4]Ko, N. W. M., and Kwan, A. S. H., "The Initial Region of Subsonic Coaxial Jets," *Journal of Fluid Mechanics*, Vol. 73, Pt. 2, 1976, p. 305.

[5]Buresti, G., Petagna, P., and Talamelli, A., "Experimental Characterization of the Velocity Field of a Coaxial Jet Configuration," *Experimental, Thermal and Fluid Science*, Vol. 9, No. 2, 1994, p. 135.

[6]Lasheras, J. C., Lecuona, A., and Rodriguez, P., "Three-Dimensional Structure of the Vorticity Field in the Near Region of Laminar, Co-flowing Forced Jets," *NATO ASI Series (B)*, Vol. 268, 1992, p. 95.

[7]Dahm, W. J. A., Frieler, C. E., and Tryggvason, G., "Vortex Structure and Dynamics in the Near Field of a Coaxial Jet," *Journal of Fluid Mechanics*, Vol. 241, Aug. 1992, p. 371.

[8]Tang, S. K., and Ko, N. W. M., "Coherent Structure Interactions in an Unexcited Coaxial Jet," *Experiments in Fluids*, Vol. 17, No. 3, 1994, p. 147.

[9]Wicker, R. B., and Eaton, J. K., "Near Field of a Coaxial Jet With and Without Axial Excitation," *AIAA Journal*, Vol. 32, No. 3, 1994, pp. 542–546.

[10]Orlanski, I., "A Simple Boundary Condition for Unbounded Hyperbolic Flows," *Journal of Computational Physics*, Vol. 21, 1976, p. 251.

[11]Pauley, L. L., Moin, P., and Reynolds, W. C., "The Structure of Two-Dimensional Separation," *Journal of Fluid Mechanics*, Vol. 220, Nov. 1990, pp. 397–441.

[12]Verzicco, R., and Orlandi, P., "A Finite-Difference Scheme for the Three-Dimensional Incompressible Flows in Cylindrical Coordinates," *Journal of Computational Physics* (to be published).

[13]Kim, J., and Moin, P., "Application of a Fractional-Step Method to Incompressible Navier–Stokes Equations," *Journal of Computational Physics*, Vol. 59, No. 2, 1985, pp. 308–323.

[14]Rai, M. M., and Moin, P., "Direct Simulations of Turbulent Flow Using Finite-Difference Schemes," *Journal of Computational Physics*, Vol. 96, No. 1, 1991, pp. 15–53.

[15]Verzicco, R., Orlandi, P., and Salvetti, M. V., "Numerical Simulations of Axisymmetric Space Developing Circular Jets," Università di Pisa and Unversità di Roma (manuscript in preparation).

[16]Buresti, G., and Petagna, P., private communication, Dipartimento di Ingegneria Aeroepaziale, Università di Pisa, 1994.

[17]Davis, R. W., and Moore, E. F., "A Numerical Study of Vortex Merging in Mixing Layers," *Physics of Fluids*, Vol. 28, 1985, pp. 1626–1635.

[18]Maekawa, H., Mansour, N. N., and Buell, J. C., "Instability Mode Interactions in a Spatially Developing Plane Wake," *Journal of Fluid Mechanics*, Vol. 235, Feb. 1992, pp. 223–254.

[19]Akselvoll, K., and Moin, P., "Large Eddy Simulation of Turbulent Confined Coannular Jets and Turbulent Flow over a Backward Facing Step," Thermosciences Div., Dept. of Mechanical Engineering, Rept. No. TF-63, Stanford Univ., Stanford, CA, Feb. 1995.

[20]Jin, G., and Braza, M., "A Nonreflecting Outlet Boundary Condition for Incompressible Navier–Stokes Calculations," *Journal of Computational Physics*, Vol. 107, No. 2, 1993, pp. 239.

[21]Dai, Y., Kobayashi, T., and Taniguchi, N., "Large Eddy Simulation of Plane Turbulent Jet Flow Using a New Outflow Velocity Boundary Condition," *Japan Society of Mechanical Engineers International Journal*, Series B, Vol. 37, No. 2, 1994.

[22]Sutherland, B. R., and Peltier, W. R., "Turbulence Transition and Internal Wave Generation in Density Stratified Jets," *Physics of Fluids*, Vol. 3, No. 6, 1994, p. 1267.

[23]Buell, J. C., and Huerre, P., "Inflow/Outflow Boundary Conditions and Global Dynamics of Spatial Mixing Layers," *Proceedings of the Summer Program*, Center for Turbulence Research, Stanford Univ., Rep. CTR-588, Stanford, CA, 1988.

[24]Chong, M. S., Perry, E., and Cantwell, B. J., "A General Classification of Three-Dimensional Flow Fields," *Physics of Fluids A*, Vol. 5, No. 2, 1990, p. 765.

[25]Verzicco, R., and Orlandi, P., "Mixedness in the Formation of a Vortex Ring," *Physics of Fluids*, Vol. 7, No. 6, 1995, p. 1513.

[26]Rogers, M. M., and Moser, R. D., "The Three-Dimensional Evolution of a Plane Mixing Layer: The Kelvin–Helmholtz Rollup," *Journal of Fluid Mechanics*, Vol. 243, Oct. 1992, p. 183.

[27]Moser, R. D., and Rogers, M. M., "The Three-Dimensional Evolution of a Plane Mixing Layer: Pairing and Transition to Turbulence," *Journal of Fluid Mechanics*, Vol. 247, Feb. 1993, p. 275.

[28]Verzicco, R., and Orlandi, P., "Direct Simulations of the Transitional Regime of a Circular Jet," *Physics of Fluids A*, Vol. 6, No. 2, 1994, p. 751.